Anal. Chem. **2010,** *82,* 9549–9556

High-Aspect-Ratio, Silicon Oxide-Enclosed Pillar Structures in Microfluidic Liquid Chromatography

Lisa C. Taylor,[†] Nickolay V. Lavrik,*[,‡] and Michael J. Sepaniak*[,†]

Department of Chemistry, University of Tennessee, Knoxville, Tennessee 37996, United States, and Center for Nanophase Materials Sciences, Oak Ridge National Laboratory, Oak Ridge, Tennessee 37830, United States

The present paper discusses the ability to separate chemical species using high-aspect-ratio, silicon oxide-enclosed pillar arrays. These miniaturized chromatographic systems require smaller sample volumes, experience less flow resistance, and generate superior separation efficiency over traditional packed bed liquid chromatographic columns, improvements controlled by the increased order and decreased pore size of the systems. In our distinctive fabrication sequence, plasma-enhanced chemical vapor deposition (PECVD) of silicon oxide is used to alter the surface and structural properties of the pillars for facile surface modification while improving the pillar mechanical stability and increasing surface area. The separation behavior of model compounds within our pillar systems indicated an unexpected hydrophobic-like separation mechanism. The effects of organic modifier, ionic concentration, and pressure-driven flow rate were studied. A decrease in the organic content of the mobile phase increased peak resolution while detrimentally effecting peak shape. A resolution of 4.7 (RSD = 3.7%) was obtained for nearly perfect Gaussian shaped peaks, exhibiting plate heights as low as 1.1 and 1.8 μm for fluorescein and sulforhodamine B, respectively. Contact angle measurements and DART mass spectrometry analysis indicate that our employed elastomeric soft bonding technique modifies pillar properties, creating a fortuitous stationary phase. This discovery provides evidence supporting the ability to easily functionalize PECVD oxide surfaces by gas-phase reactions.

Recent research has indicated that advances in on-chip separation technology can be gained by adapting fabrication practices similar to those developed for the semiconductor industry. Current processing techniques have the ability to decrease defined geometries to nanoscale dimensions with nanometer accuracy, thereby becoming well-suited for lab-on-chip platforms. In addition to the open channel geometries prevalent in nanochromatography applications,[1−5] recent research has focused on creating chromatographic supports integrated within fluidic channels.[6−9] This alternative approach to packed bed chromatography, first proposed by Regnier et al.,[10,11] introduced the concept of creating pillar arrays within channels with the capability of tailoring pillar position, size, shape, and pitch in a highly controllable and ordered manner. Extensive theoretical studies[12−14] and experimental studies[15] have shown that this increased order imparts fundamental advantages over the traditional packed and monolithic columns. These improvements include eliminating the polydispersity of packing particle size and heterogeneity of the packing porosity, which limits separation efficiency. Additional advantages identified by recent studies show that nearly perfect ordered pillar arrays are highly permeable with less flow resistance than comparable traditional packed and monolithic columns.[6,12,16,17] This characteristic lends itself to the application of pressure-driven liquid chromatography.

Recent reports suggest that as characteristic dimensions of separation channels decrease, nanoscale modes of separation may arise under pressure-driven conditions. These include electrostatic-derived hydrodynamic separations[18−20] and streaming potential generated electrokinetic separations.[21−25] Additional novel separation mechanisms, like the use of deterministic lateral displacement[26] discovered for particle separation, have been performed

* Corresponding authors. E-mail: msepaniak@utk.edu (M.J.S.).
[†] University of Tennessee.
[‡] Oak Ridge National Laboratory.

(1) Phan, V. N.; Yang, C.; Nguyen, N. T. *Microfluid. Nanofluid.* **2009**, *7*, 519–530.
(2) Detobel, F.; Fekete, V.; De Malsche, W.; De Bruyne, S.; Gardeniers, H.; Desmet, G. *Anal. Bioanal. Chem.* **2009**, *394*, 399–411.
(3) Clicq, D.; Vankrunkelsven, S.; Ranson, W.; De Tandt, C.; Barn, G. V.; Desmet, G. *Anal. Chim. Acta* **2004**, *507*, 79–86.
(4) Fekete, V.; Clicq, D.; De Malsche, W.; Gardeniers, H.; Desmet, G. *J. Chromatogr. A* **2008**, *1189*, 2–9.
(5) Kato, M.; Inaba, M.; Tsukahara, T.; Mawatari, K.; Hibara, A.; Kitamori, T. *Anal. Chem.* **2010**, *82*, 543–547.
(6) Lavrik, N. V.; Taylor, L. C.; Sepaniak, M. J. *Lab Chip* **2010**, *10*, 1086–1094.
(7) De Smet, J.; Gzil, P.; Vervoort, N.; Verelst, H.; Baron, G. V.; Desmet, G. *J. Chromatogr. A* **2005**, *1073*, 43–51.
(8) Kaji, N.; Tezuka, Y.; Takamura, Y.; Ueda, M.; Nishimoto, T.; Nakanishi, H.; Horiike, Y.; Baba, Y. *Anal. Chem.* **2004**, *76*, 15–22.
(9) Sainiemi, L.; Keskinen, H.; Aromaa, M.; Luosujarvi, L.; Grigoras, K.; Kotiaho, T.; Makela, J. M.; Franssila, S. *Nanotechnology* **2007**, *18*, 505303.
(10) He, B.; Regnier, F. *J. Pharm. Biomed. Anal.* **1998**, *17*, 925–932.
(11) Regnier, F. E. *HRC-J. High Resolut. Chromatogr.* **2000**, *23*, 19–26.
(12) Schure, M. R.; Maier, R. S.; Kroll, D. M.; Davis, H. T. *J. Chromatogr. A* **2004**, *1031*, 79–86.
(13) Gzil, P.; Vervoort, N.; Baron, G. V.; Desmet, G. *Anal. Chem.* **2003**, *75*, 6244–6250.
(14) De Smet, J.; Gzil, P.; Vervoort, N.; Verelst, H.; Baron, G. V.; Desmet, G. *Anal. Chem.* **2004**, *76*, 3716–3726.
(15) Eghbali, H.; Verdoold, V.; Vankeerberghen, L.; Gardeniers, H.; Desmet, G. *Anal. Chem.* **2009**, *81*, 705–715.
(16) De Malsche, W.; Eghbali, H.; Clicq, D.; Vangelooven, J.; Gardeniers, H.; Desmet, G. *Anal. Chem.* **2007**, *79*, 5915–5926.
(17) De Pra, M.; De Malsche, W.; Desmet, G.; Schoenmakers, P. J.; Kok, W. T. *J. Sep. Sci.* **2007**, *30*, 1453–1460.
(18) Wang, X. Y.; Kang, J. Z.; Wang, S. L.; Lu, J. J.; Liu, S. R. *J. Chromatogr. A* **2008**, *1200*, 108–113.

10.1021/ac1023342
Published on Web 10/28/2010

by manipulating pillar positions to impart separation by altering the path taken by varying particles. In traditional packed bed liquid chromatography, a stationary phase is distributed onto solid supports for a mobile phase−stationary phase partitioning-based separation, governed by a solute's retentive behavior within the system.

Among the few applications of pressure-driven separations previously explored for pillar array systems, modification of the pillar supports by a hydrophobic reverse phase stationary component is the most common. Desmet and co-workers have conducted impressive chromatographic separations using C8 and C18 liquid phase modifications of both porous[27] and nonporous[16,28,29] pillar arrays. While these experiments have clearly demonstrated the feasibility of applying this emerging technology to real world samples, they have also identified fundamental and practical challenges that must be addressed for these chip-level devices to be able to progress toward competing with traditional packed bed HPLC columns.

First, to achieve the same mass loadability as conventional HPLC columns, lab-on-chip devices will require geometries or treatments that would increase the surface area available for chromatographic exchange. Theory provides convincing evidence of the advantages gained with the use of high surface area porous pillar arrays.[13,14] Recent innovations by Malsche et al.[30] and Tiggelaar et al.,[31] who introduced the use of electrochemical anodization to create porous silicon shell pillars, were highly successful in increasing the surface area of pillar arrays. However, they also sacrificed the mechanical stability of high-aspect-ratio pillars fabricated in this manner. Second, liquid-phase functionalization of pillar surfaces is not trivial, as it is an intensive and timely procedure that has a poor success rate for usable devices due to the frequency of occlusion.[28] We report, herein, efforts to meet these challenges.

In our previous work[6] we introduced a fabrication sequence that implemented ordered high-aspect-ratio pillar arrays as a robust, uniquely sealed network of pores integrated into a system of fluidic channels. These enclosed systems increased the mechanical stability of the pillars. This allows for pillar diameters to be scaled down to 1 μm or less, having aspect ratios of approximately 20:1, while maintaining the ability to withstand damages potentially incurred during processing, handling, and sealing of the devices. The pillar arrays were tested for chromatographic efficiency and produced plate heights (H) as low as 0.7 μm.

In this study, we build upon our earlier work and further analyze the effect of this enclosure procedure on the separation characteristics of the pillar system. Examination into the pillar side walls produced during this fabrication sequence shows that this streamlined fabrication process produces beneficial surface characteristics for improving mass loadability as well as stationary phase functionalization. This includes generating roughened side walls absent of deep pores, thereby increasing surface area without creating deep nonswept voids that can detrimentally contribute to band variances caused by resistance to mass transfer in the stationary phase. In this respect, the pillars also act similar to core−shell type materials in which the packing structure decreases the average path length of retained solute particles during the diffusion process.[32,33] In addition, the nature of the PECVD silicon oxide is known to increase surface silanol concentrations for facile stationary phase functionalization. As an alternative to liquid-phase functionalization, Mery et al. demonstrated a vapor-phase silane procedure that made the chip coatings process more efficient and eliminated the clogging issues.[34] Herein we analyze a serendipitous gas-phase modification accomplished by the elastomeric cover window components. The retentive behavior of two model fluorescent compounds is studied.

EXPERIMENTAL SECTION

Channel Fabrication. Fabrication of the fluidic chips with an integrated injection system and enclosed silicon oxide layer was performed using the method described in our previous work.[6] The fabrication sequence involved photolithographic processing of both the front side (fluidic channels including three inlet ports orientated in a cross junction with a single straight channel, approximately 10 mm long ×50 μm wide, leading to a single outlet port) and back side (through-wafer access ports) of a standard silicon wafer. In the first step, the front side pattern was defined using a double-layer resist system (LOR 1A followed by 955CM-2.1, MicroChem Corp.) and standard contact UV photolithography (Quintel, Inc.). A 15 nm Cr masking layer (Electron beam dual gun evaporation chamber, Thermonics Laboratory) followed by subsequent lift-off procedures yielded a final hard masked design for etching. Anisotropic deep reactive ion etching (DRIE) of the channel and pillar design was performed using a Bosch process (System 100 plasma etcher, Oxford Instruments).

To create the capping layer, the front side processing was completed by deposition of a nonconformal layer of silicon oxide with a nominal thickness of 2−3 μm using plasma-enhanced chemical vapor deposition (PECVD, Oxford Instruments). For back side processing a 2 μm PECVD silicon oxide hard mask plus photoresist (SPR 220−4.5 MicroChem Corp.) was photolithographically patterned with through-wafer ports. DRIE of first the silicon oxide and then the silicon (using a modified Bosch process) in the exposed area created access ports etched entirely through the wafer for liquid introduction during experimentation.

(19) Wang, X. Y.; Wang, S. L.; Veerappan, V.; Byun, C. K.; Nguyen, H.; Gendhar, B.; Allen, R. D.; Liu, S. R. *Anal. Chem.* **2008**, *80*, 5583–5589.
(20) Wang, X. Y.; Cheng, C.; Wang, S. L.; Zhao, M. P.; Dasgupta, P. K.; Liu, S. R. *Anal. Chem.* **2009**, *81*, 7428–7435.
(21) Pennathur, S.; Santiago, J. G. *Anal. Chem.* **2005**, *77*, 6772–6781.
(22) Mansouri, A.; Scheuerman, C.; Bhattacharjee, S.; Kwok, D. Y.; Kostiuk, L. W. *J. Colloid Interface Sci.* **2005**, *292*, 567–580.
(23) Morikawa, K.; Mawatari, K.; Kato, M.; Tsukahara, T.; Kitamori, T. *Lab Chip* **2010**, *10*, 871–875.
(24) Xuan, X. C. *Anal. Chem.* **2007**, *79*, 7928–7932.
(25) Xuan, X. C.; Sinton, D. *Microfluid. Nanofluid.* **2007**, *3*, 723–728.
(26) Huang, L. R.; Cox, E. C.; Austin, R. H.; Sturm, J. C. *Science* **2004**, *304*, 987–990.
(27) De Malsche, W.; Gardeniers, H.; Desmet, G. *Anal. Chem.* **2008**, *80*, 5391–5400.
(28) Eghbali, H.; De Malsche, W.; Clicq, D.; Gardeniers, H.; Desmet, G. *LC·GC Eur.* **2007**, *20*, 208.
(29) Eghbali, H.; Matthijs, S.; Verdoold, V.; Gardeniers, H.; Cornelis, P.; Desmet, G. *J. Chromatogr. A* **2009**, *1216*, 8603–8611.
(30) De Malsche, W.; Clicq, D.; Verdoold, V.; Gzil, P.; Desmet, G.; Gardeniers, H. *Lab Chip* **2007**, *7*, 1705–1711.
(31) Tiggelaar, R. M.; Verdoold, V.; Eghbali, H.; Desmet, G.; Gardeniers, J. G. E. *Lab Chip* **2009**, *9*, 456–463.
(32) Gritti, F.; Leonardis, I.; Abia, J.; Guiochon, G. *J. Chromatogr. A* **2010**, *1217*, 3819–3843.
(33) Cavazzini, A.; Gritti, F.; Kaczmarski, K.; Marchetti, N.; Guiochon, G. *Anal. Chem.* **2007**, *79*, 5972–5979.
(34) Mery, E.; Ricoul, F.; Sarrut, N.; Constantin, O.; Delapierre, G.; Garin, J.; Vinet, F. *Sensors Actuators, B* **2008**, *134*, 438–446.

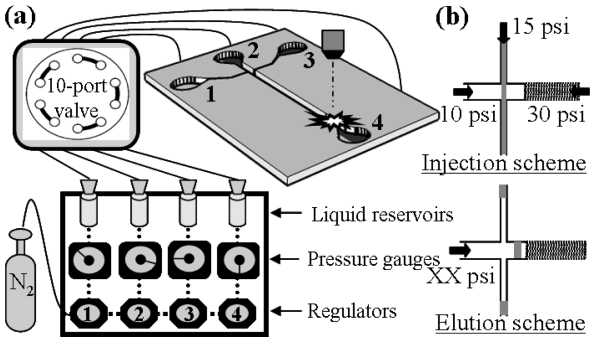

Figure 1. (a) Simplified schematic illustration of the experimental setup. (b) Sample injection and elution scheme for manipulating pressurized flow generation.

Experimental Setup and Separation Procedure. The fluidic interface that coupled the fabricated chips with off chip components is analogous to the design described in our earlier work.[6] Modifications to the previous design were aimed at constructing a more compact system to become more compatible with the overall goal of system miniaturization. Figure 1a depicts the main components of our experimental setup. In short, we designed a homemade pressurized system that was operated by connecting a nitrogen gas cylinder to precision regulators (Airtrol Components Inc.) that attenuated the pressure fed to four liquid reservoirs. The flow generation at each reservoir was additionally controlled by a 10-port valve (Valco Instruments Co. Inc.) that provided switching between sample injection and elution flow regimes, as described by the protocol in Figure 1b. The assembled fluidic chip was mounted onto an adapter directly attached to the microscope stage for epifluorescent detection.

Prior to performing separations and functional tests on the system, the chips were bonded to elastomeric cover windows to create sealed fluidic devices. For this procedure, glass cover slides of the same dimension of the chips were first spin-coated with approximately 25 μm of polyethylene glycol modified GE RTV 615 [10:1 parts A:B ratio with 0.4% polyethylene glycol−methyl ether methacrylate (PEG−MEM)] and cured at 100 °C for 1 h. Afterward, the cover window and fluidic chip were placed into contact and heated on a hot plate at 90 °C for 5 min. The resulting device was thus reversibly sealed, so that once attached to the adapter the fluidic system could withstand pressures up to 100 psi and once released from the adapter the cover window could be manually removed and the chip easily washed and reused.

To visualize sample injection and characterize chromatographic separations, a Nikon Eclipse 100 microscope equipped with a high-pressure Hg light source, a multicolor filter cube, and a Digital sight CCD camera (DS-2M, Nikon, Inc.) controlled by NIS-Elements software was used. Separations were conducted using fluorescein sodium salt (Sigma Aldrich) and sulforhodamine B (Acros Organics) laser dye with various compositions of solvent mixtures containing methanol and phosphate buffer (pH 8).

Surface and Phase Characterization. The properties of the pillar array created during the fabrication process were inspected by collecting images using an FEI Dual Beam SEM/FIB (xT Nova Nanolab 200). HPLC experiments were completed using a HP series 1100 HPLC. Capillary electrophoresis experiments were conducted on a Hewlett-Packard 3D CE using a 75 μm id capillary. Contact angles were measured using a Rame-Hart NRL contact angle goniometer (model 100). Stationary-phase characterization was conducted using an Ion Sense DART 100 mass spectrometer coupled to a JEOL AccuTOF JMS-T100LC.

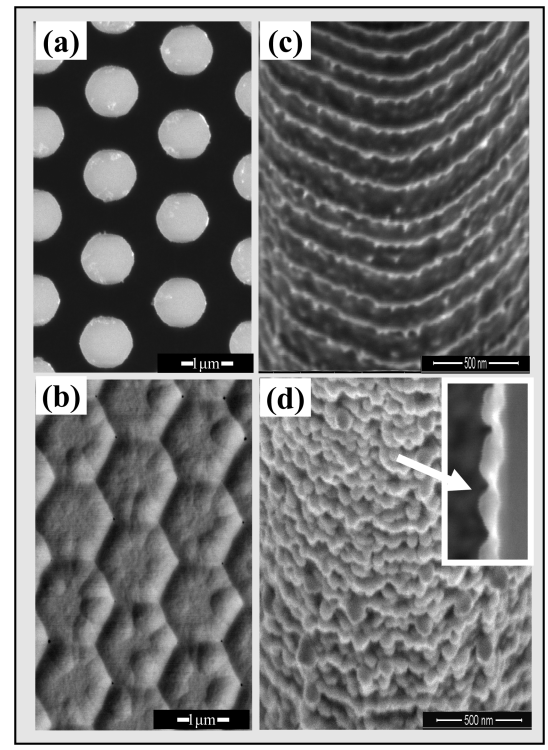

Figure 2. SEM images illustrating the pillar array before and after the PECVD silicon oxide capping layer: (a and b) top view of pillars before and after deposition and (c and d) view of pillar side walls before and after deposition, respectively. (Inset of d) Cross sectional view of pillar side wall with oxide deposition (denoted by arrow).

RESULTS AND DISCUSSION

Channel Fabrication. The optimization of our fabrication method was explored in our previous publication.[6] The established processing sequence, continued in this study, generates fluidic chips with a 10 mm × 50 μm channel of robust 1 μm diameter pillars with a pitch of 2 μm in a 20 μm deep channel, intrinsically establishing greater surface area per pillar than previously reported nonporous pillars due to the extreme high-aspect-ratio dimensions. The major advantage of this employed system is the introduction of an oxide deposition which functions to both improve mechanical stability and impart unique surface characteristics that are studied in this work. The SEM images depicted in Figure 2 show the pillar array before and after the PECVD silicon oxide capping layer. The PECVD process produces a slightly nonstoichiometric silicon oxide with a compositional formula close to SiO_2 with a relatively high silanol content in the bulk. Deposition parameters including substrate temperature, RF power level, reactor pressure, and reactant gas flow rates affect the composition and structure of the growing film by altering the deposition process. We made adjustments to these parameters, most significantly by increasing deposition pressure, to create a nonconformal deposition that preferentially deposits oxide on the tops of the pillars.

Parts a and b of Figure 2 are top view images of the pillar array before and after the deposition of silicon oxide, respectively. As the gaps between the pillars decrease, the oxide creates a

mushroom-capped array of pillars that eventually becomes completely sealed, creating a robust scaffold that prevents delicate pillars from being damage. The enhanced mechanical stability was evident in our ability to handle, wash, seal, reseal, and even sonicate the fluidic chips without damaging the integrity of the pillars. This improved strength also allows for the ability to scale the pillars to nanoscale dimensions and very high-aspect-ratios without sacrificing the mechanical stability of the system. As pillar dimensions decrease, the effective surface area of the system increases within given channel geometries, i.e., imparting a greater surface area to volume ratio. The protective oxide enclosure also allows for facile chip sealing. A major advantage of lab-on-chip technology is the ability to use and discard these relatively inexpensive devices. However, as these pillar arrayed fluidic channels are a relatively new field, further experimentation and optimization must be conducted before adaptation as economical competitive real world systems. Our technological approach benefits from a quick and easy bonding technique that allows for chip reusability and is more forgiving of nonuniform surface topography, so that our devices are sealed with a near perfect success rate.

Parts c and d of Figure 2 depict images of the pillar side walls before and after silicon oxide deposition, respectively. As seen in Figure 2c, the anisotropic Bosch etching method creates ridges due to the unique two-step cycling protocol. The Bosch process consists of alternating etch and deposition cycles, in which the deposition step coats the feature with a fluoropolymeric layer, preventing lateral etching by radicals, and the etchant step removes the polymer for the bottom of the feature, etching the underlying silicon.[35] Typically, the polymeric layers remaining on the features side walls are removed with heat and acid washing procedures.[16,28] With our process we are able to neglect this cleaning step and instead coat this unwanted layer with silicon oxide. The deposition-to-etch ratio effects the overall etch rate and resultant feature characteristics such as established thickness of the polymer layer and the ability to maintain straight side walls without the undercutting of features. Our pillar system is created with a 5 s deposition to 4 s etch ratio, which is optimized for small diameter pillars and gives a high density of ridge features.

The ridges alone do not impart a large increase in surface area per pillar; however, when combined with the nanoscale dimensions of the pillar system and the nature of the silicon oxide deposition, these characteristics create an arrangement of high-aspect-ratio roughened pillars with increased surface area, as seen in Figure 2d. Figure 2d (inset) depicts the typical pillar cross section highlighting the additive effect of the Bosch produced ridges with the nonconformal silicon oxide deposition (approximately 70 nm thick, denoted by arrow) on the pillar side wall. Without consideration of surface roughness, our current configuration (50 μm $\times$ 1 cm array) has approximately the same surface area to volume ratio as a 3 μm i.d. open capillary while providing more than 2 orders of magnitude higher volumetric flow and concomitant related relaxed injection and detection volume demands. Our preliminary BET studies and analysis by SEM imaging suggest that the surface area of these pillars is likely to be increased by a roughness factor of up to 10 due to the presence

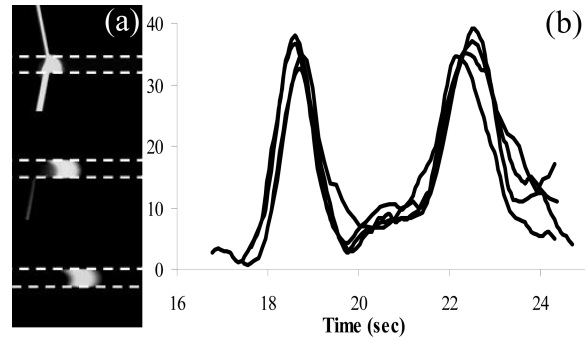

Figure 3. (a) Fluorescent micrographs of sample injection. (b) Reproducibility of chromatograms (four repeated analyses) manually injected at 30 psi. Other conditions: mobile phase composition 20:80 methanol: 50 μM phosphate buffer (pH 8); sample composition 10:90 methanol: 50 μM phosphate buffer (pH 8), 1 $\times$ 10^{-3} M fluorescein (peak 1), and 5 $\times$ 10^{-4} M sulforhodamine B (peak 2).

of PECVD silicon oxide. Previous studies have shown that PECVD silicon oxides are more porous, less uniform, and more silanol rich in comparison to dense stoichiometric silicon oxide films prepared by thermal oxidation of single crystal silicon. The silanol concentration of such films are between 1 and 6 wt %, with values changing according to deposition temperature, pressure, and RF power level.[36] In conventional electronic applications, these attributes are detrimental to the quality of the resultant film; however, in our application, these key features enhance pillar surface properties. Specifically, after PECVD of silicon oxide, the pillar sidewalls have a granular morphology with increased surface area and an increased content of silanol groups.

Functional and Chromatographic Testing. Recognizing that our injection system is manually operated, we aimed to validate the reproducibility of our experimental setup. Figure 3a shows progressive microscope images of the fluorescent solutes injected into the fluidic channel using the pressure scheme previously described. A major problem associated with on-chip injection valves is that diffusion and poorly controlled flow often results in cross contamination between inlets and downstream flow.[37] This was evident in our studies, as samples injected after an appreciable length of eluent flow produced immediate sample plugs of differing fluorescent intensity. We therefore used simultaneous variation of the pressure applied to different inlets, as depicted in Figure 1b, to be able to load the sample plug into the cross section for up to 20 min. This maintained the integrity of the sample composition and concentration, reliably producing low picoliter sample plug volumes. Figure 3b shows the reproducibility of the chromatographic separations using this injection system. Sample plugs were injected into the separation channel by varying the sample loading time (approximately 1−10 min) and the time between injections (approximately 2−12 min) with a continuous mobile phase pressure of 30 psi. The relative standard deviation of the detected peak areas was approximately 2% and 7% for fluorescein and sulforhodamine B, respectively, while peak resolution had a relative standard deviation of less than 7%. These results

(35) Craigie, C. J. D.; Sheehan, T.; Johnson, V. N.; Burkett, S. L.; Moll, A. J.; Knowlton, W. B. *J. Vac. Sci. Technol. B* **2002**, *20*, 2229–2232.

(36) Ceiler, M. F.; Kohl, P. A.; Bidstrup, S. A. *J. Electrochem. Soc.* **1995**, *142*, 2067–2071.

(37) Braschler, T.; Theytaz, J.; Zvitov-Marabi, R.; Van Lintel, H.; Loche, G.; Kunze, A.; Demierre, N.; Tornay, R.; Schlund, M.; Renaud, P. *Lab Chip* **2007**, *7*, 1111–1113.

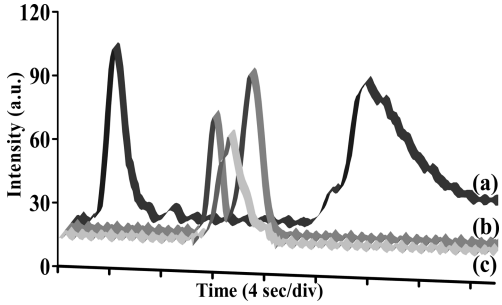

Figure 4. Chromatograms of fluorescein and sulforhodamine B using a mobile phase composition of (a) 40:60 methanol:buffer, (b) 20:80 methanol:buffer, and (c) 10:90 methanol:buffer systems. Other conditions: 50 μM phosphate buffer (pH 8); sample composed of 30:70 methanol:buffer, 5×10^{-4} M sulforhodamine B, and 1×10^{-3} M fluorescein; eluent pressure of 30 psi.

indicate that the experimental setup used for our studies is suitable for future analyses.

To evaluate the separation performance of our fluidic devices, we examined the behavior of two large organic compounds compatible with our detection system, fluorescein (FW 376.3) and sulforhodamine B (FW 558.67). The elution order of the separated compounds using our pillar array system was fluorescein then sulforhodamine B. This trend is consistent with results collected in both our HPLC C18 reverse-phase chromatographic separations and our CE experiments. The CE results revealed that in our solvent systems (i.e., pH 8) the model compounds have electrophoretic mobilities of approximately -2×10^{-3} and -1×10^{-3} cm^2/V s for fluorescein sodium salt and sulforhodamine B, respectively, indicating that both compounds are negatively charged anions yet exhibit adequate organic character for reversed-phase HPLC retention.

Figure 4 shows the chromatograms obtained in our pillar system with variation of the composition of the mobile phase by adjusting the concentration of the organic modifier. As depicted, the chromatographic resolution between the two peaks greatly decreases with the increase of the methanol fraction. This trend indicates that some type of hydrophobic mode of retention governs the chromatographic behavior in our system. Possible separation mechanisms that act in this manner are partition-based hydrophilic interaction liquid chromatography (HILIC), a variant of normal-phase chromatography, and the more common reverse-phase chromatography (RPC). If operating in the HILIC mode, a thin layer of absorbed water would be formed on the pillar surface and charged polar analytes, such as the dye used in these experiments, would partition into and out of the absorbed water layer as well as undergo cation exchange with charged silanol groups.[38] For this mechanism to dictate the separation, the mobile phase must be highly organic.[38,39] In contrast, our separations utilize highly aqueous mobile phases, a regime that would not produce HILIC separations. We therefore determined that RPC, which would create a trend consistent with that depicted in Figure 4, is the more likely mode of separation. This is further supported by the tailing depicted in Figure 4a by the sulforhodamine B peak. In RPC, tailing may occur due to phase overload or due to interaction with exposed, free surface silanol groups. Another

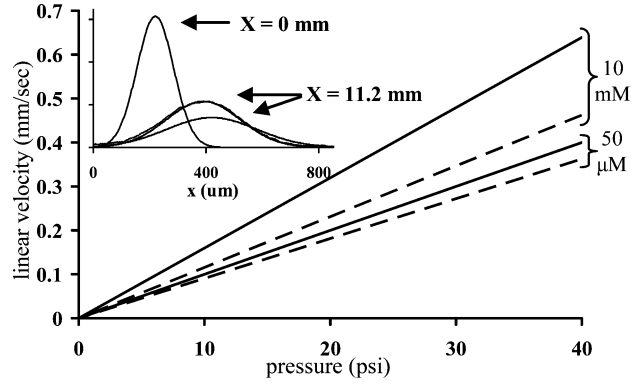

Figure 5. Relationship of solute velocity and pressure for fluorescein (solid lines) and sulforhodamine B (dashed lines) in different ionic strength buffers. (Inset) Intensity profile of injected sample pre- and postpillars using 10 mM buffer strength at 22 psi. Conditions: mobile phase composition 20:80 methanol:phosphate buffer (pH 8). Sample composed of 30:70 methanol:buffer, 5×10^{-4} M sulforhodamine B, and 1×10^{-3} M fluorescein. Peaks fit to a Gaussian, middle peak modeled with experimental and fit curves.

possible source of tailing at lower mobile phase organic content may be due to injecting the sample in a solvent stronger than the mobile phase.

The separation behavior exhibited by our system was unexpected and the exact mechanism of retention still unknown, so next we examined the effect of the ionic strength of the mobile phase, and therefore the Debye length, on the separation performance. It has been reported that an electric streaming potential can be created in nanoscale channels that ultimately imparts new separation mechanisms.[21,40–43] Studies have also shown that localization of solutes into the center of the parabolic profile may produce electrostatically derived hydrodynamic effects, wherein analytes may separate due to their differential access to the full parabolic flow profile, referred to by Liu et al. as nanocapillary chromatography.[18–20] Both of these aforementioned separation modes should result in similar separation trends with changes in ionic strength. Previous studies examining these separation mechanisms have only been applied to open channel geometries. We aimed to reproduce these experiments in our pillar packed channels to verify or eliminate the significance of these modes of separation in our systems. The plots depicted in Figure 5 show the relationship between solute velocity and pressure for given mobile phase compositions. The calculated Debye length under our conditions was approximately 3 and 40 nm for the ionic concentrations of 10 mM and 50 μM, respectively.[44,45] If there was an appreciable streaming potential, the lower ionic strength and Debye length should produce greater potential and better electrophoretic separation. The same trend should be observed with the hydrodynamic separation mechanism, wherein we would expect greater localization toward channel center and increased velocities and separation of the negatively charged analytes.[5,19] The absence of these trends (see the figure) indicates

(38) Hao, Z. G.; Xiao, B. M.; Weng, N. D. *J. Sep. Sci.* **2008**, *31*, 1449–1464.
(39) Gritti, F.; Pereira, A. D.; Sandra, P.; Guiochon, G. *J. Chromatogr. A* **2009**, *1216*, 8496–8504.
(40) Pennathur, S.; Santiago, J. G. *Anal. Chem.* **2005**, *77*, 6782–6789.
(41) Xuan, X. C. *J. Chromatogr. A* **2008**, *1187*, 289–292.
(42) Xuan, X. C.; Li, D. Q. *Electrophoresis* **2007**, *28*, 627–634.
(43) Griffiths, S. K.; Nilson, R. H. *Anal. Chem.* **2006**, *78*, 8134–8141.
(44) Qiao, R.; Aluru, N. R. *J. Micromech. Microeng.* **2002**, *12*, 625–635.
(45) Tandon, V.; Bhagavatula, S. K.; Nelson, W. C.; Kirby, B. J. *Electrophoresis* **2008**, *29*, 1092–1101.

Table 1. Effect of Ionic Concentration on the Retention Factor (k) of Fluorescein and Sulforhodamine B for Separations Performed in Our Pillar Structured Fluidic Channels and in a Traditional HPLC C18 Column

		retention factor (k)	
separation system	mobile phase ionic strength	fluorescein	10 mM sulforhodamine B
pillar array	50 μM	0	0.10
	10 mM	0	0.34
C18 HPLC	50 μM	0.59	1.18
	10 mM	0.65	2.52

that, even if present, the electric gradient and electrostatic-derived hydrodynamic effects are not the dominant mechanisms governing separations.

Figure 5, inset, illustrates the representative intensity profiles of the sample plug at injection (x = 0 mm) and detection (x = 11.2 mm) positions. Plate heights were 1.1 and 1.8 μm for fluorescein and sulforhodamine B at 22 psi, respectively. Although the slopes of the plots in Figure 5 diverge to a great extent as pressure increases, especially in the case of the 10 mM ionic concentration, this trend should not be misconstrued as increased resolution. In fact, the resolution is nearly the same for all pressures within each individual solvent system (Res = 4.7 ± 0.2, RSD = 3.7% for the 10 mM ionic strength mobile phase). Determination of the retention factor (k) from the figure yields the values described in Table 1. The elution time of the mobile phase (t_m) was determined by measuring the velocity of an unretained analyte in the 1 mm open channel prior to the pillar array. Specifically, fluorescein is unretained (thus t_m) at both ionic strengths, while sulforhodamine B exhibits modest retention under the described conditions.

To determine if these relationships are consistent with what would occur with traditional RPC, we conducted experiments similar to those described using a traditional HPLC system. The two model compounds were injected into a Varian Microsorb MV 100 C18 column (5 μm particles, 150 × 4.6 mm) at 1.5 mL/min with a 50:50 methanol:phosphate buffer mobile phase of both the 50 μM and 10 mM ionic strength. To achieve the target flow rate for the 50 μM ionic strength experiments required an approximate 145 psi increase in pressure in comparison to the 10 mM ionic strength experiments, a trend consistent with the on-chip results (Figure 5). The retention factor (k) for both solutes are listed in Table 1. The retention factor of the fluorescein was approximately equal at both ionic strengths, while it varied to a larger extent for sulforhodamine B, again consistent with the pillar system. For both systems, increasing the ionic strength of the buffer more than doubled the retention of sulforhodamine B. These results further indicate that our pillar array system operates similar to RPC, however, with less capacity than the traditional C18 HPLC column.

Phase Characterization. Clearly our native pillar system alone should not perform in a RPC mode without functionalization; thus, we sought to determine the source of this modification. We utilize an elastomeric cover window to seal our closed chip systems, resulting in an extremely confined small volume channel. This elastomeric soft bonding technique was the most obvious cause for this retentive behavior. Once in contact with a silicone substance, a substrate may assume the characteristics of the elastomer, often referred to as silicone contamination.[46−48]

Table 2. Contact Angle Measurement of Silicon Oxide Thin Film and Silicon Oxide Enclosed Pillars prior to and after Exposure to Employed Cover Windows and Elastomeric Components

treatment		contact angle, deg
native (untreated)	thin film	35.3
	pillar array	−
part A PDMS	pillar array	117.6
part B PDMS	pillar array	111.8
PEG−MEM	pillar array	−
PDMS window cured 1 h, 100 °C	thin film	77.2
	pillar array	119.8
PDMS−PEG window cured 1 h, 100 °C	thin film	95.2
	pillar array	123.5
array soaked in hexane for 4 h		120.8
array baked at 230 °C for 4 h		121.4
PDM S-PEG window cured for 10 h at 100 °C	thin film	69.6
	pillar array	−
PDMS−PEG window cured for 1 h at 100 °C + 25 °C for >30 days	thin film	61.6
	pillar array	−

Commercial PDMS networks have an excess of the silane functional cross-linking agent that plays a major role in possible chemical adhesion processes. Studies suggest that silanes (Si−H) can either bond to a surface through the hydroxyl group and cross-polymerize to form a layer or can hydrolyze to form silanol groups (Si−OH) that can form hydrogen bonds or condense with other silanol groups, forming Si−O−Si bonds.[49] In our system, the pillar structured channel where the separation occurs is capped with a protective oxide layer; therefore, it was unclear if the bonding technique affected the open channel in the same manner as the enclosed pillar array. More specifically, we wanted to ascertain if silicone contamination is due to surface contact or an effect of volatile compounds. Studies suggest that 5−20% of the elastomeric material does not undergo cross-linking reactions and only 0.1% of the total mass of the elastomer is volatile at ambient temperature and pressure.[46] We tested for gas-phase contamination by volatile components by measuring the contact angle (Table 2) of both a silicon oxide thin film as well as an array of our silicon oxide-coated pillars before and after a series of exposures to the treated elastomeric-coated cover window with and without the PEG additive, the individual elastomer components (GE RTV 615 part A PDMS and part B cross-linking agent), and the individual PEG−MEM additive. Exposure to the aforementioned cover window components was conducted by storing the chips next to the described components in the same desiccator at room temperature for approximately 48 h. Contact angle measurements were collected using the sessile drop method with a 10 μL droplet,

(46) Andersson, L. H. U.; Hjertberg, T. *J. Appl. Polym. Sci.* **2003**, *88*, 2073–2081.

(47) Andersson, L. H. U.; Johander, P.; Hjertberg, T. *J. Appl. Polym. Sci.* **2003**, *90*, 3780–3789.

(48) Hale, P. S.; Kappen, P.; Prissanaroon, W.; Brack, N.; Pigram, P. J.; Liesegang, J. *Appl. Surf. Sci.* **2007**, *253*, 3746–3750.

(49) Perutz, S.; Kramer, E. J.; Baney, J.; Hui, C. Y. *Macromolecules* **1997**, *30*, 7964–7969.

listing the results as an average of five measurements per sample. Measurements of the thin film prior to exposure revealed a contact angle of approximately 35°, whereas we were unable to even maintain a water droplet on the pillar surface due to the hydrophilic nature of PECVD silicon oxide. This result also confirms that the pillars are coated with silicon oxide rather that the fluoropolymer produced by the Bosch process, which would be extremely hydrophobic.

After exposure to key PDMS components, the contact angle increased to an extremely hydrophobic angle (see Table 2). Measurement within the array exhibited markedly higher contact angles, which is expected when measuring textured surfaces, which can trap air within the structure.[50] PEG alone did not impart contact angle change and, in turn, did not hinder the ability of the PDMS−PEG window in making the surfaces hydrophobic. We therefore hypothesize that vapor-phase elastomeric components could modify the surfaces of both the open channel as well as the pillar array enclosed by the PECVD silicon oxide capping layer. To understand if the surface modification is a result of chemical adsorption or chemical bonding, we exposed the PDMS−PEG-modified pillar array to extreme heat and solvent conditions. These treatments did not significantly alter the hydrophobic properties of the array. We assume that any adsorbed species would be baked or washed off by these procedures; thus, we concluded that the phase is most likely chemically bound to the silicon oxide surface. It should be noted that the cover windows were exposed to the array and thin film within 2 weeks of forming and curing them in the same manner used for bonding. We later tried the same experiments using months old cover windows as well as windows cured for an additional 8 h. These chips yielded no appreciable change in contact angle, especially within the pillar array. This result implies that over time the cover windows will totally degas and any volatile or non-cross-linked component will either disseminate or migrate away from the surface and into the bulk of the silicone.

Further characterization of the modified silicon oxide film was performed using mass spectrometry. As with the contact angle experiments, we collected positive ion mass spectra of each individual neat elastomeric component (part A, part B, and PEG−MEM) and of the silicon oxide film exposed to our typical cover window. Figure 6a depicts the mass spectrum of the neat component part A, while Figure 6b represents the mass spectrum of the silicon oxide film before (inset) and after exposure to a cover window we use for conducting separations. The labeled peaks differ by the repeating unit of the PDMS chain (inset of Figure 6a). Figure 6a,b shares these characteristic fragmentations; however, the other spectra collected provided no obvious direct similarities to that of the spectrum collected for Figure 6b. This provides some evidence that the part A component contributes to the observed surface altering effects. It should be noted that we are unable to eliminate the possibility that part B may also contribute to the phase, as many peaks collected in the spectrum were not identified. Efforts to collect a spectrum of the native film prior to surface modification with the PDMS components yielded no ionizable species (see Figure 6b, inset). These results confirm a definite surface change for our silicon oxide-coated and enclosed

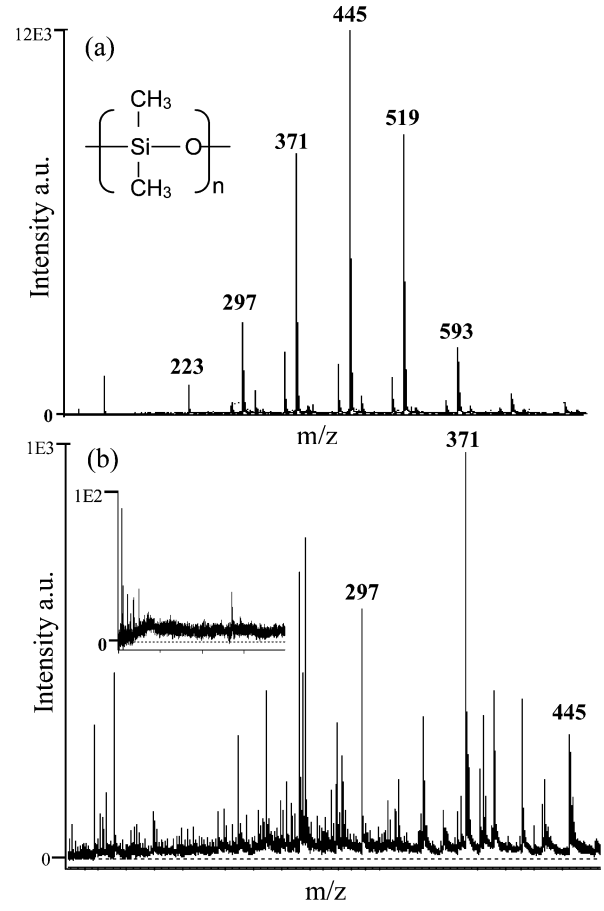

Figure 6. Positive ion mass spectrum of (a) neat part A PDMS and (b) a PDMS−PEG modified and unmodified (inset) silicon oxide film.

system, where our employed elastomeric bonding method inherently creates a phase that ultimately imparts hydrophobic-like separation characteristics. It should be noted that while we believe gas-phase silicone contamination dominates the stationary phase modification, liquid-phase contamination of the mobile phase during experimental use may also occur.

To determine the homogeneousness of the PDMS coating within the pillar array, we measured the velocity of the most retained component (sulforhodamine B) at three different locations along the pillar bed. The band velocity had a RSD value of 12.6%. This indicated that the stationary-phase coating within the pillar bed was sufficiently homogeneous. We would expect any short-range heterogeneity of the PDMS coating to manifest as decreased band and separation efficiency. However, as previously stated, plate heights (H) of less than 2 μm and reproducible chromatograms (Figure 3) were obtained.

CONCLUSION

Lab-on-chip chromatographic systems offer fundamental advantages over traditional separation media, as they require minute volumes, decreasing sample and reagent waste; they attain extremely fast analysis times, achieving improved efficiency with a small footprint; and they can be produced at a fraction of the cost. However, to realize the full potential of pillar arrays as competitive chip-based separation systems improvements are needed to increase the mechanical stability, surface area, and

(50) Callies, M.; Chen, Y.; Marty, F.; Pepin, A.; Quere, D. *Microelectron. Eng.* **2005**, *78−79*, 100–105.

operational characteristics of the devices. We have developed a unique fabrication sequence for creating robust high-aspect-ratio pillar array separation channels that improves pillar integrity and increases pillar surface area.

Separations were carried out under pressure-driven flow conditions using an elastomeric bonding technique that allows for facile sealing and chip reusability. Silicone contamination by this bonding method produced a reverse-phase chromatographic separation with an apparent small phase ratio. This outcome suggests that a much simpler method for modifying these systems could be gas-phase reactions rather than the more complicated liquid-phase reactions commonly used. In these current studies, this modification process was unintentional; however, future studies will focus on using silylating agents with high vapor pressures to create deliberate stationary phases for chromatographic separations.

ACKNOWLEDGMENT

A portion of this research at Oak Ridge National Laboratory's Center for Nanophase Materials Sciences was sponsored by the Scientific User Facilities Division, Office of Basic Energy Sciences, U.S. Department of Energy. Special thanks to Stephen Gibson and the UTK Center for Mass Sepctrometry and Dr. Bin Zhao for assistance with sample analysis.

Received for review September 2, 2010. Accepted October 18, 2010.

AC1023342